Discovery of a Potent, Selective, and Orally Bioavailable Pyridinyl-Pyrimidine Phthalazine Aurora Kinase Inhibitor

Victor J. Cee,*[†] Laurie B. Schenkel,[†] Brian L. Hodous,[†] Holly L. Deak,[†] Hanh N. Nguyen,[†] Philip R. Olivieri,[†] Karina Romero,[†] Annette Bak,[‡] Xuhai Be,[§] Steve Bellon,[∥] Tammy L. Bush,[⊥] Alan C. Cheng,[∥] Grace Chung,[⊥] Steve Coats,[⊥] Patrick M. Eden,[⊥] Kelly Hanestad,[⊥] Paul L. Gallant,[#] Yan Gu,[∥] Xin Huang,[∥] Richard L. Kendall,[⊥] Min-Hwa Jasmine Lin,[§] Michael J. Morrison,[#] Vinod F. Patel,[†] Robert Radinsky,[⊥] Paul E. Rose,[∥] Sandra Ross,[#] Ji-Rong Sun,[⊥] Jin Tang,[∥] Huilin Zhao,[∥] Marc Payton,[⊥] and Stephanie D. Geuns-Meyer[†]

Departments of [†]*Medicinal Chemistry,* [‡]*Pharmaceutics,* [§]*Pharmacokinetics and Drug Metabolism,* [∥]*Molecular Structure,* [⊥]*Oncology Research,* and [#]*Molecular Pharmacology, Amgen Inc., 360 Binney Street, Cambridge, Massachusetts 02142 and Amgen Inc., One Amgen Center Drive, Thousand Oaks, California 91320*

The discovery of aurora kinases as essential regulators of cell division has led to intense interest in identifying small molecule aurora kinase inhibitors for the potential treatment of cancer. A high-throughput screening effort identified pyridinyl-pyrimidine **6a** as a moderately potent dual inhibitor of aurora kinases -A and -B. Optimization of this hit resulted in an anthranilamide lead (**6j**) that possessed improved enzyme and cellular activity and exhibited a high level of kinase selectivity. However, this anthranilamide and subsequent analogues suffered from a lack of oral bioavailability. Converting the internally hydrogen-bonded six-membered pseudo-ring of the anthranilamide to a phthalazine (**8a−b**) led to a dramatic improvement in oral bioavailability (38−61%*F*) while maintaining the potency and selectivity characteristics of the anthranil-amide series. In a COLO 205 tumor pharmacodynamic assay measuring phosphorylation of the aurora-B substrate histone H3 at serine 10 (p-histone H3), oral administration of **8b** at 50 mg/kg demonstrated significant reduction in tumor p-histone H3 for at least 6 h.

Introduction

The aurora family of serine/threonine kinases is represented by three paralogous genes (aurora-A, -B, and -C).[1] Aurora-A and -B are essential mitotic regulators required for chromosome alignment, segregation, and cytokinesis, while aurora-C function appears to be restricted mainly to spermatogenesis. Despite the high degree of structural similarity, aurora-A and -B have distinct subcellular localizations and functions during mitosis. As cells enter mitosis, aurora-A is localized to the centrosomes and the proximal mitotic spindle, whereas aurora-B is localized to the kinetochore/centromeric region. At the onset of anaphase, as sister-chromatids separate, aurora-B localizes to the spindle midzone where it coordinates exit from mitosis.[1,2] Aurora-A can function as an oncogene capable of transforming rodent fibro-blast cells in culture.[1,3] Expression of aurora-A and -B is elevated in a variety of human cancers, with increased expression corre-lating with poor prognosis in many cases.[1,4]

In tumor cells, inhibition of aurora-B or dual inhibition of aurora-A and -B leads to premature exit from mitosis, result-ing in undivided 4N DNA-containing cells in the G_1-phase of the cell cycle. These cells can progress through further rounds of genome replication without cellular division, a process referred to as endoreduplication, which ultimately results in cell death.[1] The described mechanism of action for an aurora-A/B kinase inhibitor is distinct from that of traditional antimitotic agents in that death of tumor cells is driven by continued cell-cycle progression rather than by arrest in mitosis (e.g., paclitaxel and docetaxel).

A considerable research effort from both the pharmaceu-tical industry and academic laboratories has led to many reports of small molecule aurora kinase inhibitors.[5] Both pan-aurora kinase inhibitors and subtype-selective inhibitors are currently under evaluation in human clinical trials. The earliest example of a pan-aurora kinase inhibitor in clinical development was MK-0457 (VX-680) (**1**), which inhibits aurora-A and -B as well as a number of other kinases implicated in cancer (Figure 1).[5] The earliest examples of isoform-selective aurora kinase inhibitors in clinical develop-ment are MLN8054, an aurora-A selective inhibitor (**2**),[6] and AZD-1152 (**3a**), a phosphate prodrug of the selective aurora-B inhibitor **3b**.[7] Herein we report the discovery of a pyridinyl-pyrimidine series of pan-aurora kinase inhibitors and describe the optimization of this series, which culminated in phthala-zine **8b**, a potent and selective inhibitor of aurora-A and -B with properties suitable for oral dosing.

Chemistry

Pyridinyl-pyrimidine chloride derivative **4**[8] was reacted with 4-aminophenol or a substituted 4-aminophenol in the presence of cesium carbonate at elevated temperature to produce penultimate aniline intermediates **5a−c** (Scheme 1). These aniline intermediates (**5a−c**) were converted to amides by HATU-mediated[a] reactions with a variety of carboxylic

---

*To whom correspondence should be addressed. Phone: 805-313-5500. Fax: 805-480-1337. E-mail: vcee@amgen.com.

[a] Abbreviations: ATP, adenosine triphosphate; Cl, clearance; HATU, *O*-(7-azabenzotriazol-1-yl)-*N,N,N′,N′*-tetramethyluronium hexafluoro-phosphate; HTS, high throughput screening; KDR, kinase insert do-main receptor; RLM, rat liver microsome; Tie-2, tyrosine kinase with extracellular epidermal growth factor homology domains 2; TPX2, targeting protein for *Xenopus* plus end-directed kinesin-like protein 2.

Scheme 1. Preparation of Amide Targets[a]

5a R^1 = R^2 = H
5b R^1 = Me, R^2 = H
5c R^1 = H, R^2 = Me

6a-6l
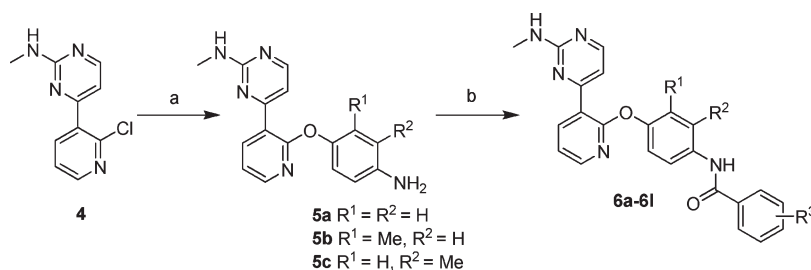
[a] Reagents and conditions: (a) 4-aminophenol, Cs$_2$CO$_3$, DMSO, 130 °C (90−95%); (b) ArCO$_2$H, HATU, DIPEA, CHCl$_3$, rt (33−84%).

Scheme 2. Preparation of Phthalazine Targets[a]

8a R$_1$ = H
8b R$_1$ = F
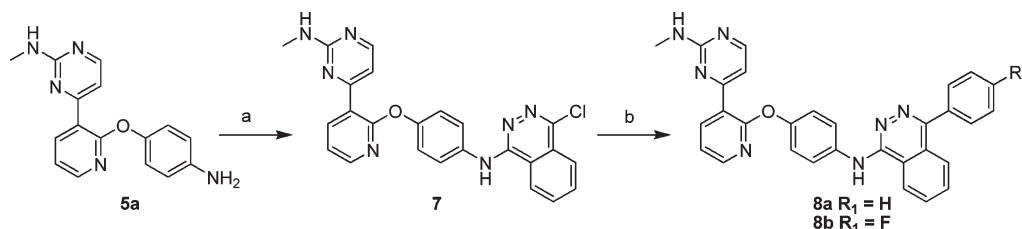
[a] Reagents and conditions: (a) 1,4-dichlorophthalazine, *s*-BuOH, 100 °C (88%); (b) boronic acid, Pd(dppf)Cl$_2$, aq Na$_2$CO$_3$, dioxane, 100 °C (44−60%).
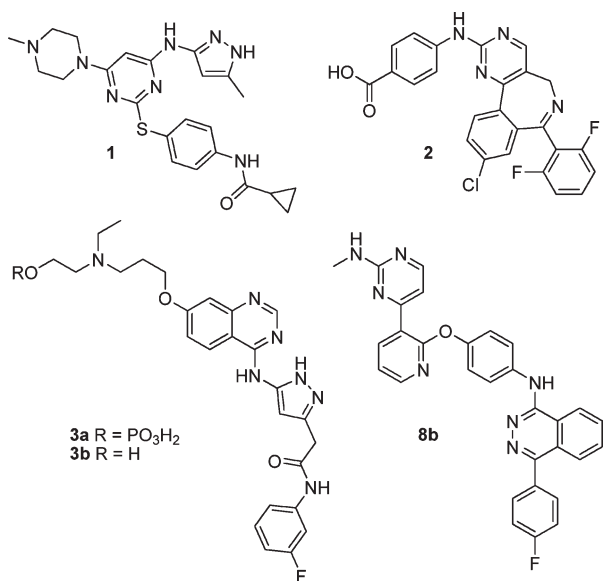

Figure 1. Representative aurora kinase inhibitors and pyridinyl-pyrimidine phthalazine **8b**.

acids to give target amides **6a**−**6l**. Phthalazines **8a** and **8b** were also derived from intermediate **5a**, which was treated with 1,4-dichlorophthalazine to provide chloride **7**. Suzuki reaction of **7** with phenyl- or 4-fluorophenylboronic acid provided **8a** and **8b**, respectively (Scheme 2).

Discussion

High throughput screening (HTS) of a kinase-focused proprietary compound collection identified pyridinyl pyrimidine amide **6a** as a moderately potent inhibitor of both aurora-A/TPX2 (aurora-A in complex with a fragment [1−43] of partner protein TPX2[9]) and aurora-B enzymes, with a reasonable level of selectivity against a small panel of kinases (Table 1). In an aurora-B cellular assay (hereafter termed 24 h DNA ploidy)
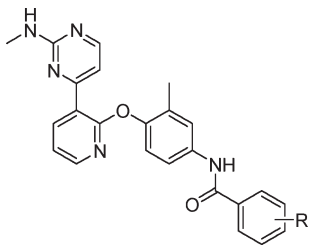
Table 1. Potency and Selectivity Summary for HTS Hit **6a**

enzyme IC$_{50}$ (nM)[a]			
aurora-A/TPX2	586	c-kit	1350
aurora-B	66	c-fms	1580
Lck	385	KDR	3270
Abl	503	Src	5750
Tie-2	630	p38α	8000

IC$_{50}$ > 8000 nM: EGFR, EphB4, IGFR-1, Zap70, Jak2, Jak3, BTK, JNK2, p70s6, PLK1, Erk1, PKBα, CDK5.

[a] All kinase assays were run at the K_m for ATP and represent an average of at least two determinations. For statistical analysis of averaged data, see the Supporting Information.

measuring the ability of a test compound to induce an accumulation of cells with ≥4N DNA content, compound **6a** was not able to increase the number of HeLa cells with ≥4N DNA content relative to control in a 24 h time period at concentrations up to 1200 nM. Therefore, our initial goal was to improve the aurora cellular potency of the screening hit **6a**.

Table 2 illustrates selected structure−activity relationships for variations of the terminal aryl ring. A positional scan of a chlorine substituent revealed that substitution at the 3- and 4-position (**6c** and **6d**) was superior to 2-substitution (**6b**), although cellular activity was still not achieved. It was hypothesized that the larger phenoxy substituent might improve inhibitory activity by increased van der Waals interactions between ligand and protein, so phenoxy-substituted analogues were also investigated. In contrast to chlorine substitution, the 2-substituted **6e** showed the most potent activity

Table 2. Potency Data for Pyridinyl-Pyrimidine Amides

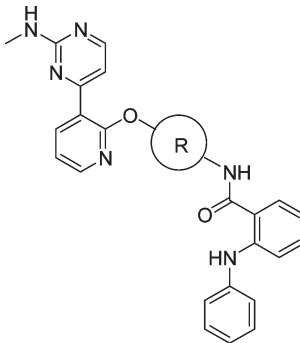| | R | enzyme, IC$_{50}$ (nM)^a | | cell, EC$_{50}$ (nM)^b |
		aurora-A/TPX2	aurora-B	DNA ploidy
6a	3-CF$_3$	586	66	>1200^c
6b	2-Cl	>25000	>25000	ND
6c	3-Cl	1546	430	>1200^c
6d	4-Cl	2342	335	>1200^c
6e	2-OPh	1544	56	>1200^c
6f	3-OPh	964	251	>1200^c
6g	4-OPh	ND	542	ND
6h	2-NHPh	62	17	89

^{a} All kinase assays were run at the K_m for ATP and represent an average of at least two determinations. ^{b} Average of at least two determinations, unless otherwise specified. ^{c} One determination. For statistical analysis of averaged data, see the Supporting Information.
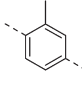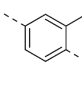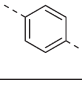
toward aurora-B enzyme in this series, although cellular activity was still not observed. Replacement of the 2-OPh substituent with 2-NHPh produced anthranilamide (**6h**), which was an important breakthrough, as this compound exhibited double-digit nanomolar potency against both aurora-A/TPX2 and aurora-B enzymes as well as an 89 nM EC$_{50}$ value in the 24 h DNA ploidy cellular assay. Although **6e** and **6h** differ by only a single atom, the conformational differences imposed by intramolecular hydrogen bonding between the ether oxygen and amide NH of salicylamide **6e** and aniline NH and carbonyl O of anthranilamide **6h** are significant, and this may contribute to the difference in potency between **6e** and **6h**.

The structure−activity relationship of the central *para*-aminophenoxy portion of the molecule is illustrated in Table 3. Moving the methyl group to the position adjacent to the aniline nitrogen (**6i**) caused a significant loss of aurora-A/TPX2 and aurora-B enzyme potency as well as poor cellular activity. Removing the methyl group (**6j**) led to an improvement in both intrinsic potency and cellular activity. These data suggest that an unsubstituted central aminophenoxy ring provides optimal potency, and further efforts focused on this series.
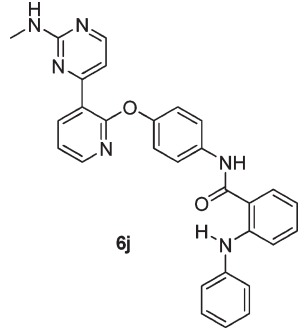
The selectivity profile of **6j** against a panel of phylogenetically diverse kinases and the pharmacokinetic properties of **6j** in Sprague−Dawley rats are presented in Table 4. Aside from aurora-A and -B, only Tie-2 and KDR enzymes were inhibited at submicromolar concentrations (IC$_{50}$ = 440 nM and 794 nM, respectively), resulting in a minimum selectivity factor of 29-fold over the EC$_{50}$ of the 24 h DNA ploidy cellular assay (440 nM against Tie-2 enzyme vs 15 nM DNA ploidy). Unfortunately, **6j** exhibited suboptimal rat pharmacokinetics, with clearance (Cl = 3.6 L/h/kg) approaching rat liver blood flow. The high clearance was consistent with rapid turnover of **6j** in rat liver microsomes (RLM Cl = 663 µL/min/mg). When dosed orally, **6j** was not detectable in rat plasma, indicating a lack of oral bioavailability.

Two fluorinated anthranilamide analogues, **6k** and **6l** (Table 5), were synthesized in order to assess the impact of

Table 3. Potency Data for Pyridinyl-Pyrimidine Anthranilamides

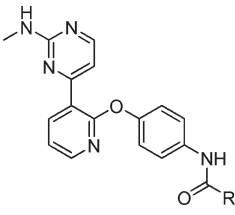| | | Enzyme, IC$_{50}$ (nM)^a | | Cell, EC$_{50}$ (nM)^b |
#	R	Aurora-A/TPX2	Aurora-B	DNA Ploidy
6h		62	17	89^c
6i		>1,000	110	1,450
6j		16	9	15

^{a} All kinase assays were run at the K_m for ATP and represent an average of at least two determinations. ^{b} Average of at least two determinations, unless otherwise specified. ^{c} One determination. For statistical analysis of averaged data, see the Supporting Information.
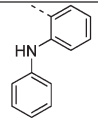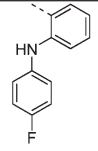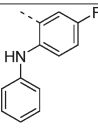
Table 4. Potency, Selectivity, and Pharmacokinetic Properties of **6j**

6j

Enzyme IC$_{50}$ (nM)^a	
aurora-A/TPX2	16
aurora-B	9
Tie2	440
KDR	794

IC$_{50}$ > 1000 nM: p38α, JNK2, cMET, Jak3, c-kit, Src, Lck, Abl(T315I), BTK, IGFR-1, CDK1, CDK2, CDK5, PKBα, p70s6k, PLK1, Erk1

Rat Pharmacokinetics^b	
Cl (L/h/kg)	3.6
Vss (L/kg)	4.8
$t_{1/2}$ (h)	2.8
%F	<1

^{a} All kinase assays were run at the K_m for ATP and represent an average of at least two determinations. ^{b} Administered intravenously at 0.5 mg/kg and orally at 2 mg/kg to male Sprague−Dawley rats (N = 3).

blocking two likely sites of oxidative metabolism.[10] Both analogues maintained comparable potency to **6j** and showed lower rates of rat liver microsome metabolism (**6k**, RLM Cl = 467 µL/min/mg, and **6l**, RLM Cl = 338 µL/min/mg). A

Table 5. Potency, Pharmacokinetic Properties, and Solubility of Anthranilamide Analogues

Compound	R	DNA Ploidy EC$_{50}$ (nM)^a	RLM (µL/min/mg)	Rat Cl (L/h/kg)^b	Rat %F^b	Solubility^c (mg/mL)
6j		15	663	3.6	<1	0.005
6k		28	467	1.6	ND	0.023
6l		20	338	0.87	<1	0.016

^{a} Average of at least two determinations; for statistical analysis of averaged data, see the Supporting Information. ^{b} Administered intravenously at 0.5 mg/kg and orally at 2 mg/kg to male Sprague−Dawley rats (N = 3). ND = not determined. ^{c} Equilibrium solubility determined in 0.01 N HCl.

corresponding reduction in clearance was also observed following iv dosing in rat, with **6l** characterized by a clearance of 0.87 L/h/kg. Unfortunately, moderating the in vitro metabolism and lowering the in vivo clearance in this series did not result in any improvement in oral bioavailability (**6l**, F < 1%), suggesting that poor absorption was likely responsible for the lack of oral bioavailability of **6l**. This was further substantiated by equilibrium solubility measurements, which established that **6l** exhibited poor solubility in aqueous media (0.016 mg/mL, 0.01 N HCl).

Figure 2 illustrates X-ray cocrystal structures of **9**[11] and **10**,[12] two analogues representative of the cell-inactive initial screening hit **6a** and the cell-active anthranilamide derivative **6j**, respectively, bound to the ATP site of the aurora-A kinase domain.[13] In the aurora-A/**9** cocrystal structure (PDB ID: 3O50), the ligand binds with the activation loop in a DFG-in conformation[14] and the terminal trifluoromethyl group is flanked by lipophilic side-chain residues of the C-helix (Val174 and Ile178) and P-loop (Phe144). Key hydrogen-bonding interactions exist between the pyrimidine nitrogen and kinase hinge NH (Ala213), the amide carbonyl and the amino terminus of the catalytic lysine (Lys162), and the amide NH of the ligand and the side chain of Asn261 (water-mediated). The cocrystal structure of aurora-A/**10** (PDB ID: 3O51) shows a similar orientation in the ATP-binding site, but the conserved DFG motif of the activation loop occupies a strikingly different DFG-out conformation, with the aromatic ring of the anthranilamide partially occupying the space vacated by Phe275 and the terminal phenyl ring flanked by lipophilic side-chain residues of the C-helix (Val174 and Ile178) and P-loop (Phe144). The anthranilamide adopts an internally hydrogen-bonded conformation, with the plane of the amide nearly parallel to Phe275. While the amide carbonyl oxygens of **9** and **10** occupy very similar space, Lys162 is disordered in the aurora-A/**10** structure, precluding any assessment of a hydrogen-bond-
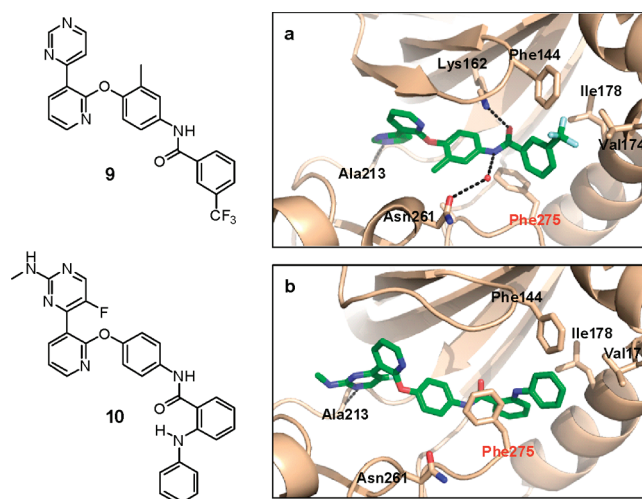
Figure 2. X-ray cocrystal structure of representative inhibitors bound to the kinase domain of aurora-A. (a) Benzamide **9**; (b) anthranilamide **10**.

ing interaction. The conformation of the kinase activation loop in the aurora-A/**10** cocrystal structure appears to be induced by the anthranilamide, as the *N*-phenyl portion of the molecule is incompatible with the protein conformation observed in the aurora-A/**9** cocrystal structure.

The aurora-A/**10** cocrystal structure verified that the anthranilamide portion of the molecule adopts a pseudo-six-membered ring conformation with an intramolecular hydrogen bond. This information supported the replacement of the pseudo-ring with a six-membered aromatic ring. Gratifyingly, phthalazine **8a**, a corollary to anthranilamide **6j**, and the *para*-fluoro derivative **8b**, a corollary to anthranilamide **6k**, demonstrated good cellular

Table 6. Emergence of the Phthalazine Inhibitors from Anthranilamide **6j**
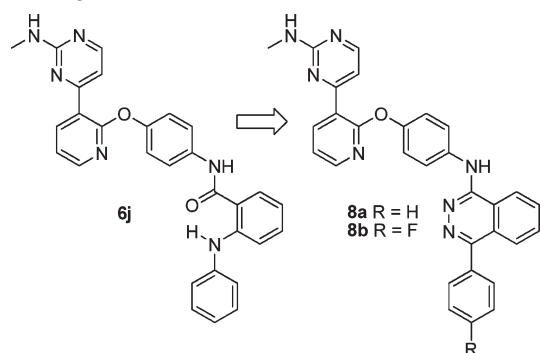
	enzyme, IC$_{50}$ (nM)^a		cell, EC$_{50}$ (nM)^b	solubility (mg/mL)
	aurora-A/TPX2	aurora-B	DNA ploidy	0.01 N HCl
6j	16	9	15	0.005
8a	149	22	15	0.159
8b	41	15	24	>0.200

^{a} All kinase assays were run at the K_m for ATP and represent an average of at least two determinations. ^{b} Average of at least three determinations. For statistical analysis of averaged data, see the Supporting Information.

Table 7. Pharmacokinetic Properties of **8a** and **8b**^{a}

	Cl (L/h/kg)	Vss (L/kg)	$t_{1/2}$(h)	%F
8a	0.80	0.69	1.3	61
8b	0.44	0.42	1.1	38

^{a} Administered intravenously at 0.5 mg/kg and orally at 2 mg/kg to male Sprague−Dawley rats ($N = 3$).

potency (Table 6). Both **8a** and **8b** show significantly improved solubility in aqueous media (0.01 N HCl) versus **6j**, and both were selected for rat pharmacokinetic experiments. Both **8a** and **8b** (Table 7) showed significantly lower clearance as well as greatly improved oral bioavailability relative to the anthranilamides **6j** and **6l** (Table 5).

Compound **8b** was further profiled against a panel of diverse kinases (Table 8). Aside from aurora-A and -B, only Tie-2 and p38α enzymes were inhibited with IC$_{50}$ values less than 25 μM (IC$_{50}$ = 872 nM and 1700 nM, respectively), resulting in a minimum selectivity factor of 36-fold over the EC$_{50}$ of the 24 h DNA ploidy cellular assay (872 nM against Tie-2 enzyme vs 24 nM 24 h DNA ploidy).

The impact of **8b** on aurora kinase function was further established by experiments in the human cervical cancer cell line HeLa. Exposure of synchronized cells to **8b** (0.0049 to 5 μM) and measurement of phosphorylated aurora-A (Thr 288) and aurora-B (Thr 232) by Western blotting revealed near-complete suppression of p-aurora-A and p-aurora-B at 0.313 μM **8b** (Figure 3A). In this experiment, 0.5 μM MLN8054 (**2**, aurora-A kinase

Table 8. Kinase Selectivity of **8b**^{a}

enzyme	IC$_{50}$ (nM)
aurora-A/TPX2	41
aurora-B	15
Tie-2	872
p38α	1700
IC$_{50}$ > 25000 nM: KDR, Lck, Src, BTK, IGFR-1, Jak3, JNK2, CDK5, Erk1, c-Met, p706s6k, PLK1, PKBα, PKBβ, MSK1, Abl(T315I), c-Kit	

^{a} All kinase assays were run at the K_m for ATP and represent an average of at least two determinations.
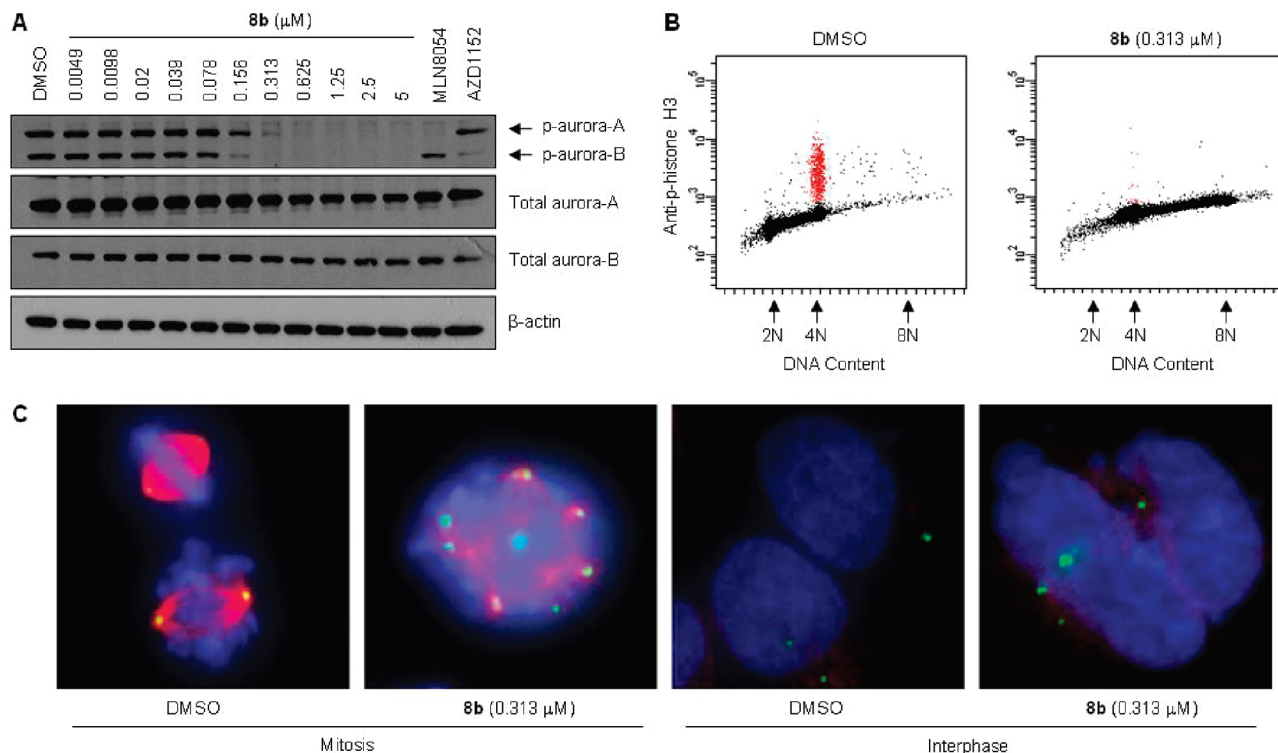
Figure 3. Compound **8b** inhibits aurora-A and aurora-B activity and induces polyploidy in human tumor cells. (A) Western blotting of cell lysates from HeLa cells synchronized in mitosis and treated with DMSO, compound **8b** at the indicated concentrations, MLN8054 (aurora-A kinase inhibitor) at 0.5 μM, or AZD1152 (aurora-B kinase inhibitor) at 1 μM for 3 h. (B) HeLa cells were treated with DMSO or **8b** at 0.313 μM for 24 h. The levels of p-histone H3 Ser 10 (red) and DNA content (2N, 4N, and 8N) were determined by flow cytometry. (C) Representative merged images of HeLa cells treated with DMSO or compound **8b** at 0.313 μM for 48 h. Cells were immunostained with anti-α-tubulin (red) and anti-pericentrin (green) antibodies and DNA counterstained with DAPI (blue).

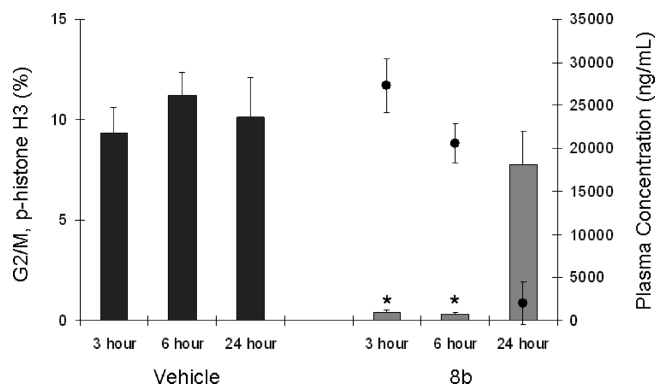**Figure 4.** Mice bearing established COLO 205 xenograft tumors were administered a single oral dose of vehicle alone or **8b** at 50 mg/ kg. Tumors were collected at 3, 6, and 24 h after treatment ($N = 4$ per time-point) and the level of p-histone H3 was determined by immunofluorescence-based flow cyotmetry. Pharmacodynamic response is represented as the percentage of p-histone H3 positive cells in G2/M (bars, mean + SD) plotted against concentration of **8b** in mouse plasma (●) (mean ± SD). The controls (black columns) represent vehicle-treated tumors. Statistical significance was determined using ANOVA followed by Scheffe's post hoc analysis ($*P < 0.0001$ vs vehicle-treated control).

inhibitor)[6] and 1 μM AZD1152 (**3a**, aurora-B kinase inhibitor)[7] selectively blocked the autophosphorylation of either aurora-A or aurora-B, respectively, as expected. Flow cytometry experiments (Figure 3B) established that HeLa cells incubated with 0.313 μM **8b** had reduced phosphorylation of histone H3 on Ser 10 (a proximal substrate of aurora-B) and an increased percentage of cells with >4N DNA content, a direct measure of polyploidy. To investigate the effects of **8b** on cellular morphology, HeLa cells were treated with compound for 48 h and stained with DAPI (4′,6-diamidino-2-phenylindole) and antibodies to α-tubulin and to percentrin. As anticipated with inhibition of aurora-B, **8b** treatment increased the nuclear size of mitotic and interphase cells and induced irregular spindle geometry (Figure 3C). Although cell viability studies were not conducted with **8b**, our general experience with pyridinyl-pyrimidine phthalazines like **8b** is that inhibition of cell proliferation correlates well with inhibition of histone H3 phosphorylation.[15]

On the basis of excellent potency, selectivity, and acceptable rat pharmacokinetics, **8b** was selected for further evaluation in a tumor pharmacodynamic assay (Figure 4). To assess whether **8b** can inhibit phosphorylation of the aurora-B substrate histone H3 at serine 10 in vivo, mice with established COLO 205 xenograft tumors of ∼300 mm³ were orally administered a single dose of vehicle or **8b** at 50 mg/kg ($N = 12$ per group). At 3, 6, and 24 h post-treatment ($N = 4$ per time-point), plasma samples were collected and analyzed for **8b**, and tumor tissues were harvested and analyzed for p-histone H3 by immunofluorescence-based flow cytometry. After 3 and 6 h, **8b** treatment resulted in statistically significant inhibition of p-histone H3 at 50 mg/kg (≥96% inhibition, $P \leq 0.0001$) with plasma concentrations of **8b** ≥20000 ng/mL (≥38 μM). By 24 h, p-histone H3 returned to baseline levels with a plasma concentration of **8b** equal to 2460 ng/mL (4.8 μM). A qualitatively similar result was also observed in mouse bone marrow (data not shown). As **8b** is highly bound to mouse plasma proteins (>99.9% bound), the unbound concentration at the 6 h time point is <20 ng/mL (<39 nM), similar in magnitude to the DNA ploidy EC_{50} (24 nM), while the unbound concentration at the 24 h time point is <2.5 ng/mL (<5 nM), at least 5-fold below the DNA ploidy EC_{50}. The impact of **8b** on tumor growth inhibition was

not assessed, but our experience with related pyridyl-pyrimidine phthalazines indicates that ≥6 h/day suppression of tumor p-histone H3 results in robust inhibition of tumor growth.[15]

Conclusion

The evolution of a pyridinyl-pyrimidine phthalazine series of aurora kinase inhibitors has been described in detail. Structure–activity relationship studies beginning with benzamide **6a**, a dual inhibitor of aurora-A and -B with poor cellular activity, led to the discovery of anthranilamide **6j**. This lead was also a dual aurora inhibitor that displayed potent cellular activity ($EC_{50} =$ 15 nM) and good kinase selectivity. An X-ray cocrystal structure of close analogues of **6a** and **6j** bound to aurora-A revealed that the cell-inactive benzamides bind aurora-A with the kinase activation loop in a DFG-in conformation, whereas the cell-active anthranilamides bind aurora-A with the kinase activation loop in a DFG-out conformation. Lead anthranilamide **6j** exhibited high clearance and a lack of oral bioavailability in rat, and whereas improvements in in vivo clearance were possible, our ability to advance the anthranilamide series was ultimately hindered by poor oral bioavailability. Converting the internally hydrogen bonded, six-membered pseudo-ring of the anthranilamide (**6j**) to a phthalazine (**8a**−**b**) led to an unexpected improvement in equilibrium solubility in aqueous media (0.01 N HCl), reduced in vivo clearance, and a significant improvement in oral bioavailability (from <1% to ≥38% F). In addition, this phthalazine series maintained the desirable cell potency and high kinase selectivity of the anthranilamide series. In a COLO 205 tumor pharmacodynamic assay measuring phosphorylation of the aurora-B substrate histone H3 at serine 10 (p-histone H3), oral administration of **8b** at 50 mg/kg demonstrated significant reduction in tumor p-histone H3 for at least 6 h. The phthalazine series marks a significant breakthrough for the program and further optimization of this series will be reported in due course.

Experimental Section

Unless otherwise noted, all materials were obtained from commercial suppliers and used without further purification. Anhydrous solvents were obtained from Aldrich and used directly. All reactions involving air- or moisture-sensitive reagents were performed under a nitrogen or argon atmosphere. Silica gel chromatography was performed using either glass columns packed with silica gel (200−400 mesh, Aldrich Chemical) or medium pressure liquid chromatography (MPLC) on a Combi-Flash Companion (Teledyne Isco) with RediSep normal-phase silica gel (35−60 μm) columns and UV detection at 254 nm. Preparative reversed-phase HPLC was performed on a Gilson (215 liquid handler), YMC-Pack Pro C18, 150 mm × 30 mm I. D. column, eluting with a binary solvent system A and B using a gradient elusion (A: H_2O with 0.1% TFA; B: CH_3CN with 0.1% TFA) with UV detection at 254 nm. All final compounds were purified to ≥95% purity as determined by Agilent 1100 series high performance liquid chromatography (HPLC) with UV detection at 254 nm (method A: Zorbax SB-C8, 4.6 mm × 150 mm, 15 min; 1.5 mL/min flow rate; 0−100% 0.1% TFA in CH_3CN/0.1% TFA in H_2O; method B: Phenomenex Synergi, 2 mm × 50 mm, 3 min, 1.0 mL/min flow rate, 5−95% 0.1% formic acid in CH_3CN/0.1% formic acid in H_2O). NMR spectra were determined with either a Bruker AV-400 (400 MHz) spectrometer or a Varian 400 MHz or a 300 MHz spectrometer at ambient temperature. Low-resolution mass spectral (MS) data were determined on an Agilent 1100 series LCMS with UV detection at 254 nm and a low resonance electrospray mode (ESI). Chemical shifts are reported in ppm from the solvent resonance (DMSO-d_6 2.49 ppm). Data are reported as

follows: chemical shift, multiplicity (s = singlet, d = doublet, t = triplet, q = quartet, br = broad, m = multiplet), coupling constants, and number of protons. High-resolution mass spectra (HRMS) were obtained on a high resonance electrospray time-of-flight mass spectrometer.

4-(2-(4-Aminophenoxy)pyridin-3-yl)-*N*-methylpyrimidin-2-amine (5a). 4-Aminophenol (1.50 g, 13.6 mmol) was combined with cesium carbonate (8.90 g, 27.2 mmol) in DMSO (18 mL) at 100 °C for 5 min. 4-(2-Chloropyridin-3-yl)-*N*-methylpyrimidin-2-amine (**4**, 3.00 g, 13.6 mmol) was added, and the mixture was heated at 130 °C for 16 h. The cooled mixture was diluted with water, and the resulting precipitate was filtered, washed with water, and dried to yield 3.75 g (94%) of the title compound as a light-brown solid. ^{1}H NMR (300 MHz, DMSO-d_6) δ 8.40 (br s, 1H), 8.35 (d, J = 5.4 Hz, 1H), 8.15 (m, 1H), 7.30 (m, 1H), 7.21 (m, 2H), 6.82 (m, 2H), 6.58 (m, 2H), 4.98 (s, 1H), 2.86 (d, J = 4.8 Hz, 3H). MS: m/z 280.1 ([M + H]$^+$).

4-(2-(4-Amino-2-methylphenoxy)pyridine-3-yl)-*N*-methylpyrimidin-2-amine (5b). Following the procedure for **5a**, **4** and 4-amino-2-methylphenol provided the title compound (1.56 g, 90%). ^{1}H NMR (400 MHz, DMSO-d_6) δ 8.42 (br s, 1H), 8.37 (d, J = 4.0 Hz, 1H), 8.14−8.12 (m, 1H), 7.31 (d, J = 4.0 Hz, 1H), 7.21−7.18 (m, 1H), 7.13−7.11 (m, 1H), 6.72 (d, J = 8.0 Hz, 1H), 6.47−6.41 (m, 2H), 4.87 (br s, 2H), 2.88 (d, J = 4.0 Hz, 3H), 1.92 (s, 3H). MS: m/z 294.1 ([M + H]$^+$).

4-(2-(4-Amino-3-methylphenoxy)pyridine-3-yl)-*N*-methylpyrimidin-2-amine (5c). Following the procedure for **5a**, **4** and 4-amino-3-methylphenol provided the title compound (2.63 g, 95%), ^{1}H NMR (400 MHz, DMSO-d_6) δ 8.32 (br s, 1H), 8.35 (d, J = 4.0 Hz, 1H), 8.16−8.14 (m, 1H), 7.27 (d, J = 4.0 Hz, 1H), 7.22−7.19 (m, 1H), 7.10−7.14 (m, 1H), 6.74−6.75 (m, 1H), 6.69−6.71 (m, 1H), 6.60−6.62 (m, 1H), 4.70 (br s, 2H), 2.87 (d, J = 8.0 Hz, 3H), 2.05 (s, 3H). MS: m/z 294.1 ([M + H]$^+$).

N-(4-(3-(2-(Methylamino)pyrimidin-4-yl)pyridin-2-yloxy)phenyl)-2-(phenylamino)benzamide (6j). 4-(2-(4-Aminophenoxy)-pyridin-3-yl)-*N*-methylpyrimidin-2-amine (**5a**, 75 mg, 0.26 mmol), *N*-phenylanthranilic acid (65 mg, 0.31 mmol), and HATU (136 mg, 0.36 mmol) were combined in chloroform (2.0 mL) followed by the addition of DIPEA (0.089 mL, 0.51 mmol). The mixture was stirred at room temperature for 5 h. After concentration, the crude mixture was purified by flash chromatography (15−45% EtOAc/hex) to give 100 mg (79%) of the title compound as a light-yellow solid. ^{1}H NMR (400 MHz, DMSO-d_6) δ 10.41 (s, 1H), 9.17 (s, 1H), 8.42 (br s, 1H), 8.37 (s, 1H), 8.20 (m, 1H), 7.75 (m, 3H), 7.30 (m, 6H), 7.17 (m, 5H), 6.94 (m, 2H), 2.87 (s, 3H). HRMS (C$_{29}$H$_{24}$N$_6$O$_2$)$^+$ calcd 489.20335, found 489.20319.

N-(3-Methyl-4-(3-(2-(methylamino)pyrimidin-4-yl)pyridin-2-yloxy)phenyl)-3-(trifluoromethyl)benzamide (6a). Following the procedure described for **6j**, 3-trifluoromethylaniline and **5b** provided the title compound (60 mg, 77%) as a white solid. ^{1}H NMR (400 MHz, DMSO-d_6) δ 10.48 (s, 1H), 8.50 (br s, 1H), 8.39 (m, 1H), 8.30 (m, 2H), 8.17 (m, 1H), 7.98 (m, 1H), 7.80 (m, 1H), 7.71 (s, 1H), 7.65 (m, 1H), 7.22 (m, 3H), 7.10 (d, J = 8.8 Hz, 1H), 2.83 (d, J = 4.4 Hz, 3H), 2.09 (s, 3H). HRMS (C$_{25}$H$_{20}$F$_3$N$_5$O$_2$)$^+$ calcd 480.16419, found 480.16424.

2-Chloro-N-(3-methyl-4-(3-(2-(methylamino)pyrimidin-4-yl)-pyridin-2-yloxy)phenyl)benzamide (6b). Following the proce-dure described for **6j**, 2-chlorobenzoic acid and **5b** provided the title compound (74 mg, 56%) as an off-white solid. ^{1}H NMR (400 MHz, DMSO-d_6) δ 10.33 (s, 1H), 8.44 (br s, 1H), 8.38 (m, 1H), 8.16 (m, 1H), 8.02 (s, 1H), 7.91 (m, 1H), 7.60 (m, 4H), 7.32 (m, 1H), 7.26 (m, 1H), 7.17 (m, 1H), 7.09 (d, J = 8.8 Hz, 1H), 2.89 (d, J = 4.9 Hz, 3H), 2.09 (s, 3H). HRMS (C$_{24}$H$_{20}$ClN$_5$O$_2$)$^+$ calcd 446.13783, found 446.13923.

3-Chloro-N-(3-methyl-4-(3-(2-(methylamino)pyrimidin-4-yl)-pyridin-2-yloxy)phenyl)benzamide (6c). Following the procedure described for **6j**, 3-chlorobenzoic acid and **5b** provided the title compound (68 mg, 52%) as an off-white solid. ^{1}H NMR (400 MHz, DMSO-d_6) δ 10.48 (s, 1H), 8.42 (br s, 1H), 8.40 (m, 1H), 8.15 (m, 1H), 7.69 (m, 1H), 7.50 (m, 5H), 7.32 (m, 1H), 7.26 (m,

1H), 7.17 (m, 1H), 7.09 (d, J = 8.8 Hz, 1H), 2.89 (d, J = 4.9 Hz, 3H), 2.08 (s, 3H). HRMS (C$_{24}$H$_{20}$ClN$_5$O$_2$)$^+$ calcd 446.13783, found 446.13909.

4-Chloro-N-(3-methyl-4-(3-(2-(methylamino)pyrimidin-4-yl)-pyridin-2-yloxy)phenyl)benzamide (6d). Following the proce-dure described for **6j**, 4-chlorobenzoic acid and **5b** provided the title compound (86 mg, 65%) as an off-white solid. ^{1}H NMR (400 MHz, DMSO-d_6) δ 10.29 (s, 1H), 8.42 (br s, 1H), 8.39 (m, 1H), 8.16 (m, 1H), 8.00 (d, J = 6.3 Hz, 2H), 7.69 (m, 1H), 7.62 (m, 4H), 7.32 (m, 1H), 7.26 (m, 1H), 7.17 (m, 1H), 7.09 (d, J = 8.5 Hz, 1H), 2.88 (s, 3H), 2.08 (s, 3H). HRMS (C$_{24}$H$_{20}$ClN$_5$O$_2$)$^+$ calcd 446.13783, found 446.13927.

N-(3-Methyl-4-(3-(2-(methylamino)pyrimidin-4-yl)pyridin-2-yloxy)phenyl)-2-phenoxybenzamide (6e). Following the proce-dure described for **6j**, 2-phenoxybenzoic acid and **5b** provided the title compound (85 mg, 80%) as a white solid. ^{1}H NMR (400 MHz, DMSO-d_6) δ ppm 10.26 (s, 1 H), 8.45 (br s, 1 H), 8.38 (d, J = 5.2 Hz, 1 H), 8.15 (dd, J = 4.8, 2.0 Hz, 1 H), 7.68 (dd, J = 7.7, 1.6 Hz, 1 H), 7.62 (d, J = 2.3 Hz, 1 H), 7.46−7.54 (m, 2 H), 7.36−7.44 (m, 2 H), 7.21−7.33 (m, 3 H), 7.12−7.19 (m, 2 H), 7.08 (dd, J = 8.6, 1.0 Hz, 2 H), 7.03 (d, J = 8.6 Hz, 1 H) 6.96−7.00 (m, 1 H), 2.89 (d, J = 4.8 Hz, 3 H), 2.05 (s, 3 H). HRMS (C$_{30}$H$_{25}$N$_5$O$_3$)$^+$ calcd 504.20302, found 504.20379.

N-(3-Methyl-4-(3-(2-(methylamino)pyrimidin-4-yl)pyridin-2-yloxy)phenyl)-3-phenoxybenzamide (6f). Following the procedure described for **6j**, 3-phenoxybenzoic acid and **5b** provided the title compound (105 mg, 80%) as a white solid. ^{1}H NMR (400 MHz, DMSO-d_6) δ ppm 10.25 (s, 1 H), 8.46 (br s, 1 H), 8.39 (d, J = 4.9 Hz, 1 H), 8.17 (dd, J = 4.8, 2.0 Hz, 1 H), 7.74−7.83 (m, 1 H), 7.70 (d, J = 2.4 Hz, 1 H) 7.59−7.63 (m, 2 H), 7.57 (t, J = 7.9 Hz, 1 H), 7.40−7.48 (m, 2 H), 7.32 (d, J = 5.1 Hz, 1 H), 7.25−7.29 (m, 1 H), 7.22−7.25 (m, 1 H), 7.18−7.21 (m, 1 H), 7.14−7.18 (m, 1 H), 7.07−7.12 (m, 3 H), 2.89 (d, J = 4.8 Hz, 3 H), 2.09 (s, 3 H). HRMS (C$_{30}$H$_{25}$N$_5$O$_3$)$^+$ calcd 504.20302, found 504.20456.

N-(3-Methyl-4-(3-(2-(methylamino)pyrimidin-4-yl)pyridin-2-yloxy)phenyl)-4-phenoxybenzamide (6g). Following the proce-dure described for **6j**, 4-phenoxybenzoic acid and **5b** provided the title compound (85 mg, 80%) as a white solid. ^{1}H NMR (400 MHz, DMSO-d_6) δ ppm 10.15 (s, 1 H), 8.45 (br s, 1 H), 8.38 (d, J = 5.2 Hz, 1 H), 8.16 (dd, J = 4.8, 2.0 Hz, 1 H), 7.98−8.05 (m, 2 H), 7.70 (d, J = 2.2 Hz, 1 H), 7.58−7.63 (m, 1 H), 7.41−7.50 (m, 2 H), 7.31 (d, J = 5.1 Hz, 1 H), 7.19−7.28 (m, 2 H), 7.08−7.17 (m, 5 H), 7.06 (d, J = 8.6 Hz, 1 H), 2.88 (d, J = 4.8 Hz, 3 H), 2.08 (s, 3 H). HRMS (C$_{30}$H$_{25}$N$_5$O$_3$)$^+$ calcd 504.20302, found 504.20825.

N-(3-Methyl-4-(3-(2-(methylamino)pyrimidin-4-yl)pyridin-2-yloxy)phenyl)-2-(phenylamino)benzamide (6h). Following the procedure described for **6j**, *N*-phenylanthranilic acid and **5b** provided the title compound (75 mg, 54%) as a light-yellow solid. ^{1}H NMR (400 MHz, DMSO-d_6) δ 10.33 (s, 1H), 9.18 (s, 1H), 8.48 (br s, 1H), 8.39 (m, 1H), 8.19 (m, 1H), 7.80 (d, J = 7 Hz, 1H), 7.67 (s, 1H), 7.58 (m, 1H), 7.31 (m, 6H), 7.18 (m, 3H), 7.06 (m, 1H), 6.95 (m, 2H), 2.89 (s, 3H), 2.08 (s, 3H). HRMS (C$_{30}$H$_{26}$N$_6$O$_2$)$^+$ calcd 503.21900, found 503.21903.

N-(2-Methyl-4-(3-(2-(methylamino)pyrimidin-4-yl)pyridin-2-yloxy)phenyl)-2-(phenylamino)benzamide (6i). Following the procedure described for **6j**, *N*-phenylanthranilic acid and **5c** provided the title compound (123 mg, 84%) as a light-yellow solid. ^{1}H NMR (400 MHz, DMSO-d_6) δ 10.04 (s, 1H), 9.42 (s, 1H), 8.44 (br s, 1H), 8.37 (m, 1H), 8.23 (m, 1H), 7.89 (m, 1H), 7.30 (m, 6H), 7.16 (m, 5H), 6.95 (m, 3H), 2.87 (s, 3H), 2.23 (s, 3H). HRMS (C$_{30}$H$_{26}$N$_6$O$_2$)$^+$ calcd 503.21900, found 503.21869.

2-(4-Fluorophenylamino)-N-(4-(3-(2-(methylamino)pyrimidin-4-yl)pyridin-2-yloxy)phenyl)benzamide (6k). Following the pro-cedure described for **6j**, 2-(4-fluorophenylamino)benzoic acid and **5a** provided the title compound (35 mg, 33%) as a light-yellow solid. ^{1}H NMR (400 MHz, DMSO-d_6) δ 10.36 (s, 1H), 9.11 (s, 1H), 8.44 (br s, 1H), 8.37 (m, 1H), 8.21 (m, 1H), 7.77 (m, 3H), 7.39 (m, 1H), 7.17 (m, 10H), 6.92 (m, 1H), 2.88 (s, 3H). HRMS (C$_{29}$H$_{23}$FN$_6$O$_2$)$^+$ calcd 507.19393, found 507.19384.

5-Fluoro-*N*-(4-(3-(2-(methylamino)pyrimidin-4-yl)pyridin-2-yloxy)phenyl)-2-(phenylamino)benzamide (6l). Following the procedure described for **6j**, 4-fluoro-2-(phenylamino)benzoic acid[16] and **5a** provided the title compound (49 mg, 40%) as a light-brown solid. ^{1}H NMR (400 MHz, DMSO-d_6) δ 10.42 (s, 1H), 8.82 (s, 1H), 8.44 (br s, 1H), 8.35 (m, 1H), 8.19 (m, 1H), 7.74 (m, 2H), 7.63 (m, 1H), 7.27 (m, 6H), 7.16 (m, 5H), 6.89 (m, 1H), 2.86 (s, 3H). HRMS ($C_{29}H_{23}FN_6O_2$)[+] calcd 507.19393, found 507.19407.

4-Chloro-*N*-(4-(3-(2-(methylamino)pyrimidin-4-yl)pyridin-2-yloxy)phenyl)phthalazin-1-amine (7). 4-(2-(4-Aminophenoxy)-pyridin-3-yl)-*N*-methylpyrimidin-2-amine (**5a**, 8.0 g, 27.3 mmol) and 1,4-dichlorophthalazine (11.9 g, 60.0 mmol) and 136 mL *s*-BuOH were placed in a 350 mL pressure bottle and heated to 100 °C for 3 h. Upon cooling to ambient temperature, the solids were filtered and washed with MeOH. The crude material was triturated in CH_2Cl_2, filtered, washed with CH_2Cl_2, and air-dried to provide the title compound as a tan solid (11.0 g, 88% yield). ^{1}H NMR (400 MHz, DMSO-d_6) δ 10.30 (br s, 1H), 8.90−8.88 (m, 1 H), 8.60−8.54 (br s, 1H), 8.45 (d, *J* = 4.0 Hz, 1H), 8.31−8.30 (m, 1H), 8.27−8.25 (m, 1H), 8.19−8.17 (m, 2H), 7.82 (d, *J* = 8.0 Hz, 2H), 7.57−7.53 (m, 1H), 7.37−7.34 (m, 1H), 7.38 (d, *J* = 8.0 Hz, 2H), 2.96 (s, 3H). HRMS ($C_{24}H_{18}N_7OCl$)[+] calcd 455.12814, found 455.13341.

***N*-(4-(3-(2-(Methylamino)pyrimidin-4-yl)pyridin-2-yloxy)phenyl)-4-phenylphthalazin-1-amine (8a).** Following the procedure described for **8b**, phenylboronic acid and **7** provided the title compound (130 mg, 60%) as an off-white solid. ^{1}H NMR (400 MHz, DMSO-d_6) δ 9.33 (s, 1H), 8.69 (m, 1H), 8.51 (br s, 1H), 8.44 (m, 1H), 8.21 (s, 1H), 7.98 (m, 5H), 7.62 (m, 5H), 7.27 (m, 5H), 2.89 (s, 3H). HRMS ($C_{30}H_{23}N_7O$)[+] calcd 498.20368, found 498.20376.

4-(4-Fluorophenyl)-*N*-(4-(3-(2-(methylamino)pyrimidin-4-yl)-pyridin-2-yloxy)phenyl)phthalazin-1-amine (8b). 4-Chloro-*N*-(4-(3-(2-(methylamino)pyrimidin-4-yl)pyridin-2-yloxy)phenyl)-phthalazin-1-amine (**7**, 360 mg, 0.790 mmol), 4-fluorophenyl-boronic acid (276 mg, 1.97 mmol), and 1,1′-bis(diphenylphos-phino)ferrocene-palladium dichloride (116 mg, 0.158 mmol) were placed in a pressure bottle under nitrogen and taken up in 1,4-dioxane (3.9 mL). Aqueous sodium carbonate (2.0 M) (0.869 mL, 1.73 mmol) was added, and the reaction vessel was sealed and heated to 90 °C overnight. The reaction was cooled to ambient temperature, and the mixture was diluted with dichloro-methane and filtered through Celite. The filtrate was concentrated under reduced pressure and the residue purified by silica gel chro-matography (2−5% methanol/dichloromethane) to afford 4-(4-fluorophenyl)-*N*-(4-(3-(2-(methylamino)pyrimidin-4-yl)pyridin-2-yloxy)phenyl)phthalazin-1-amine (180 mg, 44%). ^{1}H NMR (400 MHz, DMSO-d_6) δ 9.35 (s, 1H), 8.69 (d, *J* = 12.0 Hz, 1H), 8.45 (br s, 1H), 8.40 (d, *J* = 4.0 Hz, 1H), 8.23−8.25 (m, 1H), 8.04−8.07 (m, 1H), 7.94−7.99 (m, 3H), 7.87−7.89 (m, 1H), 7.71−7.75 (m, 2H), 7.39−7.44 (m, 2H), 7.30−7.33 (m, 2H), 7.19−7.21 (m, 3H), 2.89 (d, *J* = 4, 3H). HRMS ($C_{30}H_{22}N_7OF$)[+] calcd 516.18699, found 516.19314.

Solubility Determination. Aqueous equilibrium solubility was determined according to an automated procedure.[17]

Homogenous Time-Resolved Fluorescence Enzyme Assays. IC_{50}'s for the inhibition of the aurora A/TPX2 complex, aurora B, and all other kinase enzymes for individual compounds were measured using an HTRF assay.[8] **Aurora enzyme kinase assays**. The Aurora HTRF kinase assays involved ATP dependent phosphorylation of a biotinylated substrate peptide in the presence or absence of an inhibitor. Aurora-A (a glutathione-*S*-transferase aurora-A catalytic domain fusion protein com-plexed with TPX2 [1−43][9]) was assayed at 10 nM using a biotinyl-PLK peptide substrate (1 μM) and ATP at its apparent K_m (1 μM) in 60 mM HEPES pH 7.5, 25 mM NaCl, 10 mM $MgCl$, 2 mM DTT, 0.05% BSA. Aurora-B (full-length aurora-B with N-terminal (His)$_6$) was assayed at 1 nM with biotinyl-histone H3 peptide (0.1 μM) and ATP at its apparent K_m (23 μM) in 50 mM HEPES pH 7.5, 5 mM NaCl, 0.5 mM $MgCl_2$, 0.5 mM $MnCl_2$, 2 mM DTT, 0.05% BSA. Enzyme assays were generally performed in 40 μL for 90−120 min at ambient temperature before stopping the reaction with 160 μL of a solution containing detection reagents (SA-APC at a final concentration of 0.002 mg/mL, and either europilated antipho-spho PLK (Ser[137]) antibody for aurora-A assay (0.080 nM) or antiphospho histone H3(Ser[10])(6G3) antibody for aurora-B assay (0.057 nM)) and 50 mM Tris, pH 7.5, 100 mM NaCl, 3 mM EDTA, 0.05% BSA, and 0.1% Tween 20. Antibodies were custom labeled by Perkin-Elmer Life Sciences. The assay plate was read using a BMG RUBYStar fluorescence plate reader with excitation at 320 nm and emission at 615 and 655 nm. **Other enzyme kinase assays**. Assays for other kinases were performed in a similar way as described above, varying the concentrations of enzyme, peptide substrate, and ATP added to the reaction, depending on the specific activity of the kinase and measured K_m's for the substrates.

Cellomics Aurora-B Cellular Assay (DNA Ploidy). HeLa cell line was obtained from the American Type Culture Collection. HeLa cells were plated at a density of 1.0×10^4 cells per well in a 96-well plate in 100 μL of complete media (DMEM with 10% FBS). The following day, cells were treated with DMSO or com-pound over a 10-point concentration range (0.0024−1.25 μM) with a final DMSO concentration of 0.1% in complete media. After 24 h, cells were fixed for 10 min at room temperature by adding 110 μL of 2× fixative solution (6.8% formaldehyde and 0.24% glutaraldehyde in 1× PBS). Cells were then permeabi-lized with wash buffer (0.5% Triton X-100 and 1% BSA in 1× PBS) at room temperature for 30 min. Cells were stained with 0.5 μg/mL Hoechst DNA dye (Invitrogen) and incubated at room temperature for 30 min. Cells were washed twice with 100 μL of wash buffer. The 96-well cell assay plates were ana-lyzed on an ArrayScan VTi HCS reader using a Cell-cycle V2 algorithm (Cellomics, Thermo Fisher Scientific). The percen-tage of cells with ≥4N DNA content were determined and used to generate a concentration−response curve and EC_{50} value using a four-parameter equation.

In Vitro Metabolism. The in vitro intrinsic clearances, CL_{int}, of the test compounds were determined in incubations of rat liver microsomes. The 400 μL incubations contained 0.25 mg of micro-somal protein/mL, 1 mM NADPH, 2 mM $MgCl_2$ in 50 mM potassium phosphate buffer, pH 7.4. To begin the reactions, test compounds were added to the prewarmed (37 °C) incubation mixtures at the final concentration of 1 μM. At 0, 10, 20, 30, and 40 min following addition of test compound, aliquots of incubation mixture (35 μL) were collected into an equal volume of acetonitrile + internal standard (1 μM tolbutamide). The samples were centrifuged at 3000*g* for 15 min and analyzed on a liquid chroma-tography tandem mass spectrometry system consisting of two Shimadzu LC-10AD HPLC pumps and a DGU-14A degasser (Shimadzu, Columbia, MD), a CTC PAL autoinjector (Leap Technologies, Carrboro, NC) and a API3000 LC-MSMS system. Chromatography was conducted on a Sprite Armor C18 (20 mm × 2.1 mm, 10 μm) analytical column (Analytical Sales and Products, Pompton Plains, NJ) with a 0.5 μm PEEK guard filter, using the following mobile phase gradient program: MPA = H_2O with 0.1% formic acid; MPB = acetonitrile with 0.1% formic acid; 0 min = 98% MPA, 2% MPB; 0.3 min = 98% MPA, 2% MPB; 0.7 min = 5% MPA, 95% MPB; 1.3 min = 5% MPA, 95% MPB; 1.4 min = 98% MPA, 2% MPB; 1.7 min = end of run; approximately 2 min between sample injections. For each compound, peak areas at each time point were converted to the natural log of the % remaining relative to the 0 min samples. The resulting slope of these values relative to time (*k*) was converted to in vitro $t_{1/2}$ where $t_{1/2}$ = −0.693/k. CL_{int} was calculated using the following relationship: $CL_{int} = (0.693/T_{1/2}) \times (1/0.25$ mg/mL).

Plasma Protein Binding. Mouse plasma protein binding was determined in filtered mouse plasma by ultrafiltration[18] at 37 °C with a 10 μM concentration of **8b**.

Pharmacokinetic Studies. Male Sprague−Dawley rats with surgically implanted femoral vein and jugular vein cannulae were obtained from Charles River Laboratories (Boston, MA). Animals were fasted overnight and the following day compounds were administered either by oral gavage or by intravenous bolus injection ($N = 3$ animals per study). Oral (OraPlus, pH = 2.2) formulations were made 24−48 h prior to dosing, while intravenous formulations (DMSO) were made on the day of dosing. Blood samples were collected over 24 h via jugular cannula into a heparinized tube. Following centrifugation, plasma samples were stored in a freezer to maintain −70 °C until analysis. Lithium heparinized plasma samples (50 μL) were precipitated with 100% acetonitrile containing the internal standard (IS). The supernatant was transferred into a 96-well plate, and an aliquot of 20 μL was injected onto an LC-MS/MS system. The analytes were separated by HPLC using a C-18 analytical column. The analyte ions were generated by an electrospray ionization (ESI) source and detected by a Sciex API3000 triple quadrupole mass spectrometer operated in the multiple reaction monitoring (MRM) mode. Study sample concentrations were determined from a weighted ($1/x^2$) linear regression of peak area ratios (analyte peak area/IS peak area) versus the theoretical concentrations of the calibration standards. Pharmacokinetic parameters were calculated using an Innaphase computer program Small Molecules Discovery Assay (SMDA) Watson.

Characterization of 8b on Aurora End Points in HeLa Cells. Nocodazole Block. HeLa cells were treated with 0.1 μg/mL nocodazole for 12 h. The cells were gently washed with PBS to remove the mitotic cell fraction. **Western blot analysis**. Cell lysates were processed for Western blot analysis as previously described.[19] Immunoblots were probed with the following antibodies: anti-aurora-A, anti-aurora-B (BD Biosciences), anti-p-aurora-A (Thr 288), anti-p-aurora-B (Thr 232) (Cell Signaling), and anti-β-actin (Sigma). Next, the immunoblots were probed with either anti-rabbit or anti-mouse IgG (Vectastain kit, Vector Laboratories), and the protein bands were detected using the Lightning-enhanced chemiluminescence kit from PerkinElmer. **Immunofluorescence cell staining**. HeLa cells were plated at 40000 cells per well in a 4-well LabTek chamber slide (Nalge Nunc) in 1 mL of complete media. The following day, cells were treated with DMSO or compound **8b** at 0.313 μM. After 48 h, cells were fixed and permeabilized as previously described.[19] Cells were blocked in 1 mL of wash buffer (PBS, 1% BSA, 0.2% Triton X-100 supplemented with 4 drops of horse serum (Vector Laboratories)) for 1 h at room temperature. The cells were then immunostained in wash buffer supplemented with rabbit anti-pericentrin (Abcam) and mouse anti-α-tubulin (Sigma) antibodies for 2 h at room temperature. Detection was performed with anti-mouse IgG-alexa-568 and anti-rabbit IgG-alexa-488 antibodies (Invitrogen) for 1 h at room temperature. Cells were washed and stained with 4′,6-diamidino-2-phenylindole (DAPI, Invitrogen) for 5 min at room temperature. One drop of ProLong Gold antifade (Invitrogen) was added to the chamber slides before affixing the glass coverslips. Representative images of cells were acquired with a Nikon upright microscope using a 40× objective. Images were collected and analyzed using MetaMorph software (MDS). DAPI nuclear staining (blue) was further enhanced using Photoshop CS4 (Adobe). **Cell-cycle assay**. Flow cytometry was performed on a LSRII using BD FACS Diva software (BD Biosciences). HeLa cells treated with DMSO or compound **8b** at 0.313 μM for 24 h. Cells were processed for cell-cycle analysis as previously described.[19] Cells were stained with anti-p-histone H3 (Ser 10) (Millipore) antibody and propidium iodide (BD Biosciences). To effectively detect the DNA content of polyploidy cells, the flow cytometer voltage settings were decreased to accommodate the 2N, 4N, and 8N cell populations.

COLO 205 Tumor Xenograft Pharmacodynamic Assay. Female CD 1 nude mice (4−6 weeks old) were obtained from Charles River, Inc. All mice were housed in sterilized cages, provided Sterilizable Rodent Diet 8656 (Harlan Teklad) and reverse osmosis water ad libitum and maintained under aseptic conditions in a ventilated rack system. All studies were conducted under the Amgen Animal Care and Use Committee protocol and satisfied all Association for Assessment and Accreditation of Laboratory Animal Care specifications. Human colon cancer carcinoma cells, COLO 205, were obtained from the American Type Culture Collection. Cells [2×10^6 cells/100 μL in a solution of 50% matrigel (Becton Dickenson Biosciences) in serum-free media] were injected subcutaneously on the right flank area of the mice. After tumors were allow establishment and growth (approximately 14−21 days post-injection) to an average size of ∼300 mm^3, mice were treated orally with a single dose of vehicle (OraPlus pH 2.2) or **8b** (50 mg/kg). Tumor and plasma samples were collected at 3, 6, and 24 h after treatment ($N = 4$ per time-point). Excised tumors were immediately minced into fine pieces with a razor blade and transferred into 10 mL of ice-cold cell dissociation buffer (Hank's buffer supplemented with Dispase II, collagenase V and XI, DNase I, and 1% BSA Fraction V) in a 50 mL conical tube containing a small magnetic stir bar. To facilitate tumor dissociation into a single-cell suspension, the tubes containing tumor pieces were stirred for 15 min at 37 °C. The cells were filtered through 70 μm filter and transferred into a new 50 mL conical tube. The filtered cells were centrifuged at 2000 rpm using a tabletop centrifuge for 4 min at 18 °C, and the supernatant was aspirated off the cell pellets. The cells were washed in 1 mL of Versene and transferred to 1.5 mL Eppendorf tube. To fix the cells, 800 μL of ice-cold 90% methanol was added dropwise and stored at −20 °C for at least 24 h. Before intracellular staining, the fixed cells were permeabilized with 200 μL of wash buffer (0.2% Triton X-100 and 1% BSA Fraction V in 1× PBS). Cells were stained in 200 μL of wash buffer with 4 μg/mL of anti-p-histone H3 antibody (Millipore) and 30 μL anti-cytokeratin-FITC antibody (Vector Laboratories) for 2 h at room temperature in the dark. Cells were then washed and stained with 1.5 μg/mL of anti-rabbit-Alexa 647 antibody (Invitrogen) for 45 min at room temperature in the dark. Cells were washed and counterstained with 600 μL of propidium iodide (PI) overnight at 4 °C in the dark. The samples were filtered through 35 μm cell strainer and transferred into 5 mL polystyrene flow cytometry tubes. Data was acquired using a LSRII flow cytometer running FACSDiva software. Stained cells were analyzed and gated according to DNA content and cytokeratin (human epithelial cell marker) to acquire a cell cycle profile. Tumor cells in the G2/M phase were evaluated for levels of p-histone H3. Tumors from mice treated with the vehicle alone served as the p-histone H3 staining control. The effect of **8b** on p-histone H3 was assessed by analysis of variance (ANOVA), followed by Scheffe post hoc testing using StatView 5.0 software. In all analysis, $P < 0.05$ was considered statistically significant.

Supporting Information Available: Statistical analysis of Aurora A/TPX2, Aurora B, and DNA Ploidy data. Synthesis of compound **10**. This material is available free of charge via the Internet at http://pubs.acs.org.

References

(1) (a) Fu, J.; Bian, M.; Jian, Q.; Zhang, C. Roles of aurora kinases in mitosis and tumorigenesis. *Mol. Cancer. Res.* **2007**, *5*, 1–10.

(b) Keen, N.; Taylor, S. Aurora-kinase inhibitors as anticancer agents. *Nature Rev. Cancer* **2004**, *4*, 927–936. (c) Carmena, M.; Earnshaw, W. C. The cellular geography of aurora kinases. *Nature Rev. Mol. Cell Biol.* **2003**, *4*, 842–854.

(2) (a) Ducat, D.; Zheng, Y. Aurora kinases in spindle assembly and chromosome segregation. *Exp. Cell Res.* **2004**, *301*, 60–67. (b) Ditchfield, C.; Johnson, V. L.; Tighe, A.; Ellston, R.; Haworth, C.; Johnson, T.; Mortlock, A.; Keen, N.; Taylor, S. S. Aurora B couples chromosome alignment with anaphase by targeting BubR1, Mad2, and Cenp-E to kinetochores. *J. Cell Biol.* **2003**, *161* (2), 267–280.

(3) (a) Marumoto, T.; Zhang, D.; Saya, H. Aurora-A—a guardian of poles. *Nat. Rev. Cancer* **2005**, *5*, 42–50. (b) Katayama, H.; Brinkley, W. R.; Sen, S. The aurora kinases: role in cell transformation and tumorigenesis. *Cancer Metastasis Rev.* **2003**, *22*, 451–464. (c) Bischoff, J. R.; Anderson, L.; Zhu, Y.; Mossie, K.; Ng, L.; Souza, B.; Schryver, B.; Flanagan, P.; Clairvoyant, F.; Ginther, C.; Chan, C. S. M.; Novotny, M.; Slamon, D. J.; Plowman, G. D. A homologue of Drosophila aurora kinase is oncogenic and amplified in human colorectal cancers. *EMBO J.* **1998**, *17*, 3052–3065.

(4) (a) Carvajal, R. D.; Tse, A.; Schwartz, G. K. Aurora kinases: new targets for cancer therapy. *Clin. Cancer Res.* **2006**, *12*, 6869–6875. (b) Montembault, E.; Prigent, C. Aurora kinases: therapeutic potential. *Drugs Future* **2005**, *30*, 29–37.

(5) For recent reviews, see: (a) Pollard, J. R.; Mortimore, M. Discovery and development of aurora kinase inhibitors as anticancer agents. *J. Med. Chem.* **2009**, *52*, 2629–2651. (b) Garuti, L.; Roberti, M.; Bottegoni, G. Small molecule aurora kinase inhibitors. *Curr. Med. Chem.* **2009**, *16*, 1949–1963. (c) Cheung, C. H. A.; Coumar, M. S.; Hsieh, H.-P.; Chang, J.-Y. Aurora kinase inhibitors in preclinical and clinical testing. *Expert Opin. Invest. Drugs* **2009**, *18*, 379–398.

(6) (a) Manfredi, M. G.; Ecsedy, J. A.; Meetze, K. A.; Balani, S. K.; Burenkova, O.; Chen, W.; Galvin, K. M.; Hoar, K. M.; Huck, J. J.; LeRoy, P. J.; Ray, E. T.; Sells, T. B.; Stringer, B.; Stroud, S. G.; Vos, T. J.; Weatherhead, G. S.; Wysong, D. R.; Zhang, M.; Bolen, J. B.; Claiborne, C. F. Antitumor activity of MLN8054, an orally active small-molecule inhibitor of Aurora A kinase. *Proc. Natl. Acad. Sci. U.S.A.* **2007**, *104*, 4106–4111. (b) Fancelli, D. Compounds and methods for inhibiting mitotic progression. *Expert Opin. Ther. Patents* **2006**, *16*, 1179–1182.

(7) Mortlock, A. A.; Foote, K. M.; Heron, N. M.; Jung, F. H.; Pasquet, G.; Lohmann, J.-J. M.; Warin, N.; Renaud, F.; De Savi, C.; Roberts, N. J.; Johnson, T.; Dousson, C. B.; Hill, G. B.; Perkins, D.; Hatter, G.; Wilkinson, R. W.; Wedge, S. R.; Heaton, S. P.; Odedra, R.; Keen, N. J.; Crafter, C.; Brown, E.; Thompson, K.; Brightwell, S.; Khatri, L.; Brady, M. C.; Kearney, S.; McKillop, D.; Rhead, S.; Parry, T.; Green, S. Discovery, synthesis, and in vivo activity of a new class of pyrazoloquinazolines as selective inhibitors of aurora B kinase. *J. Med. Chem.* **2007**, *50*, 2213–2224.

(8) Hodous, B. L.; Geuns-Meyer, S. D.; Hughes, P. E.; Albrecht, B. K.; Bellon, S.; Bready, J.; Caenepeel, S.; Cee, V. J.; Chaffee, S. C.; Coxon, A.; Emery, M.; Fretland, J.; Gallant, P.; Gu, Y.; Hoffman, D.; Johnson, R. E.; Kendall, R.; Kim, J. L.; Long, A. M.; Morrison, M.; Olivieri, P. R.; Patel, V. P.; Polverino, A.; Rose, P.; Tempest, P.; Wang, L.; Whittington, D. A.; Zhao, H. Evolution of a highly selective and potent 2-(pyridin-2-yl)-1,3,5-triazine tie-2 kinase inhibitor. *J. Med. Chem.* **2007**, *50*, 611–626.

(9) Bayliss, R.; Sardon, T.; Vernos, I.; Conti, E. Structural basis of aurora-A activation by TPX2 at the mitotic spindle. *Mol. Cell* **2003**, *12*, 851–862.

(10) Park, B. K.; Kitteringham, N. R.; O'Neill, P. M. Metabolism of fluorine-containing drugs. *Annu. Rev. Pharmacol. Toxicol.* **2001**, *41*, 443–470.

(11) The synthesis of **9** has been reported previously: Geuns-Meyer, S. D.; Hodous, B. L.; Chaffee, S. C.; Tempest, P. A.; Olivieri, P. R.; Johnson, R. E.; Albrecht, B. K.; Patel, V. F.; Cee, V. J.; Kim, J. L.; Bellon, S.; Zhu, X.; Cheng, Y.; Xi, N.; Romero, K.; Nguyen, H. N.; Deak, H. L. Preparation of nitrogen-heteroaryl-containing protein kinase modulators for use against cancer and other diseases. PCT Int. Appl. WO2005113494, 2005.

(12) The synthesis of **10** is detailed in the Supporting Information.

(13) (a) Liao, J. J.-L. Molecular recognition of protein kinase binding pockets for design of potent and selective kinase inhibitors. *J. Med. Chem.* **2007**, *50*, 409–424. (b) Heron, N. M.; Anderson, M.; Blowers, D. P.; Breed, J.; Eden, J. M.; Green, S.; Hill, G. B.; Johnson, T.; Jung, F. H.; McMiken, H. H.; Mortlock, A. A.; Pannifer, A. D.; Pauptit, R. A.; Pink, J.; Roberts, N. J.; Rowsell, S. SAR and inhibitor complex structure determination of a novel class of potent and specific aurora kinase inhibitors. *Bioorg. Med. Chem. Lett.* **2006**, *16*, 1320–1323. (c) Bayliss, R.; Sardon, T.; Vernos, I.; Conti, E. Structural basis of aurora-A activation by TPX2 at the mitotic spindle. *Mol. Cell* **2003**, *12*, 851–862. (d) Cheetham, G. M. T.; Knegtel, R. M. A.; Coll, J. T.; Renwick, S. B.; Swenson, L.; Weber, P.; Lippke, J. A.; Austen, D. A. Crystal structure of aurora-2, an oncogenic serine/threonine kinase. *J. Biol. Chem.* **2002**, *277*, 42419–42422. (e) Nowakowski, J.; Cronin, C. N.; McRee, D. E.; Knuth, M. W.; Nelson, C. G.; Pavletich, N. P.; Rogers, J.; Sang, B.-C.; Scheibe, D. N.; Swanson, R. V.; Thompson, D. A. Structures of the cancer-related aurora-A, FAK, and EphA2 protein kinases from nanovolume crystallography. *Structure* **2002**, *10*, 1659–1667.

(14) For references comparing DFG-in and DFG-out protein kinase conformations, see: (a) Nagar, B.; Bornmann, W. G.; Pellicena, P.; Schindler, T.; Veach, D. R.; Miller, W. T.; Clarkson, B.; Kuriyan, J. Crystal structures of the kinase domain of c-Abl in complex with the small molecule inhibitors PD173955 and imatinib (STI-571). *Cancer Res.* **2002**, *62*, 4236–4243. (b) Tokarski, J. S.; Newitt, J. A.; Chang, C. Y. J.; Cheng, J. D.; Wittekind, M.; Kiefer, S. E.; Kish, K.; Lee, F. Y. F.; Borzillerri, R.; Lombardo, L. J.; Xie, D.; Zhang, Y.; Klei, H. E. The structure of dasatinib (BMS-354825) bound to activated ABL kinase domain elucidates its inhibitory activity against Imatinib-resistant ABL mutants. *Cancer Res.* **2006**, *66*, 5790–5797. (c) Abagyan, R.; Kufareva, I. Type-II kinase inhibitor docking, screening, and profiling using modified structures of active kinase states. *J. Med. Chem.* **2008**, *51*, 7921–7932. (d) Zuccotto, F.; Ardini, E.; Casale, E.; Angiolini, M. Through the "Gatekeeper Door": Exploiting the Active Kinase Conformation. *J. Med. Chem.* **2010**, *53*, 2681–2694 For general references on kinase/inhibitor X-ray co-crystal structures, see: . (e) Cherry, M.; Williams, D. H. Recent kinase and kinase inhibitor X-ray structures: mechanisms of inhibition and selectivity insights. *Curr. Med. Chem.* **2004**, *11*, 663–673. (f) Fischer, P. M. The design of drug candidate molecules as selective inhibitors of therapeutically relevant protein kinases. *Curr. Med. Chem.* **2004**, *11*, 1563–1583. (g) Liu, Y.; Gray, N. S. Rational design of inhibitors that bind to inactive kinase conformations. *Nature Chem. Biol.* **2006**, *2*, 358–364.

(15) Manuscript in preparation.

(16) Palacios, M. L. D.; Comdom, R. F. P. Synthesis of *N*-phenylanthranilic acid derivative using water as solvent in the presence of ultrasound irradiation. *Synth. Commun.* **2003**, *33*, 1771–1775.

(17) Tan, H.; Semin, D.; Wacker, M.; Cheetham, J. An automated screening assay for determination of aqueous equilibrium solubility enabling SPR study during drug lead optimization. *J. Assoc. Lab Autom.* **2005**, 364–373.

(18) Wright, J. D.; Boudinot, F. D.; Ujhelyi, M. R. Measurement and analysis of unbound drug concentrations. *Clin. Pharmacokinet.* **1996**, *30*, 445–462.

(19) Payton, M.; Chung, G.; Yakowec, P.; Wong, A.; Powers, D.; Xiong, L.; Zhang, N.; Leal, J.; Bush, T. L.; Santora, V.; Askew, B.; Tasker, A.; Radinsky, R.; Kendall, R.; Coats, S. Discovery and evaluation of dual CDK1 and CDK2 inhibitors. *Cancer Res.* **2006**, *66*, 4299–4308.